A Fast Self-synchronizing Synchronverter Design with Easily Tuneable Parameters

Shuan Dong, Yu Christine Chen
Department of Electrical and Computer Engineering
The University of British Columbia
Vancouver, BC, Canada
Email: shuan@ece.ubc.ca, chen@ece.ubc.ca

***Abstract*—This paper proposes a fast self-synchronizing synchronverter controller design, which synchronizes the synchronverter inner voltage to the grid-side voltage without needing to measure its phase angle, prior to physical connection to the grid. The proposed design centres on the addition of a virtual resistance branch (along with a suitable coordinate transformation), which provides the controller with virtual active- and reactive-power output feedback signals during self synchronization, even though the actual outputs are zero before grid connection. The virtual resistance branch enables fast self synchronization by avoiding inductance dynamics in prevailing methods that use a virtual impedance branch. At the same time, the parameter tuning process is simplified as fewer parameters require tuning. Moreover, the effects of these parameters on synchronization dynamics are well defined. Time-domain simulations are provided to validate that the proposed controller design self synchronizes quickly and that its parameters are easily tuneable.**

I. Introduction

Ongoing efforts toward environmentally sustainable electricity generation give rise to gradual displacement of synchronous generators by renewable energy sources (RESs). Since RESs are usually connected to the grid via power-electronic converters, such as voltage source converters (VSCs), they behave differently from conventional synchronous generators and contribute less or no inertia to the grid. Also, conventional converter controllers rely on phase-locked loops (PLLs), which may lead to stability issues, especially in weak grid conditions [1]. To overcome these problems, the concept of *virtual synchronous generator* (VSG) has been proposed to control power-electronic converters so that they mimic the dynamic behaviours of synchronous generators [2]–[7]. Unlike conventional controller designs, VSGs contribute inertia to the grid, and they are independent of PLLs during normal operation, and as such mitigate PLL-related instabilities. Moreover, VSGs offer active-power frequency- and reactive-power voltage-droop controls. In this way, they help to improve power quality and enhance system stability [3].

A representative VSG-based controller design is the *synchronverter*, which does not need a PLL during normal operation. However, a PLL is still required to measure the grid-side voltage phase angle prior to connecting the power-electronic converter to the grid. This measurement is used to synchronize the synchronverter inner voltage to the grid-side voltage, and thus avoid potentially large start-up currents when physically connecting the synchronverter to the grid, which may cause damage to equipment. In order to completely remove PLLs and further simplify the controller, in this paper, we propose a synchronverter controller design that achieves fast self synchronization,[1] which would enable the "plug-and-play" feature for RESs connected to the grid via synchronverter controllers.

Due to the importance of achieving self synchronization, various designs have been proposed in the literature [4]–[8]. Existing controllers generally adopt a virtual impedance branch to generate virtual active- and reactive-power synchronverter outputs so as to provide the controller with appropriate feedback signals and to achieve self synchronization, even though the actual outputs are zero prior to grid connection. For example, [4] employs a large virtual impedance to limit the transient current flows immediately after grid connection, but this method requires time to gradually reduce the impedance to nominal values before normal operation may begin. The method in [5] begins normal operation immediately after self synchronization, since it switches off the virtual impedance branch after connection. However, at least five parameters need to be tuned via trial and error: two in the virtual impedance branch (resistance and inductance), two in the additional proportional-integral (PI) controller that achieves phase-angle synchronization, and one in the reactive-power loop (RPL). The method proposed in [6] replaces the PI controller in [5] with the *damping correction loop*, which freely adjusts damping torque by tuning only one parameter. During self synchronization, however, [6] still adopts the virtual impedance branch, which has two parameters that need to be tuned via trial and error. Moreover, the virtual inductance dynamics tend to slow down the self-synchronization process, and improperly chosen resistance and inductance values may even destabilize the system [9].

In view of the above, instead of the virtual impedance branch found in [4]–[6], this paper proposes a self-synchronizing synchronverter design that relies on a virtual resistance only, thereby removing inductance dynamics that may delay self synchronization. Since the synchronverter is designed for predominantly inductive grid conditions, we additionally leverage a suitable coordinate transformation so that the virtual resistance acts as a reactance when computing

[1] Self synchronization is the ability for the synchronverter to automatically synchronize its inner voltage to the grid-side voltage before connection without PLLs [5].

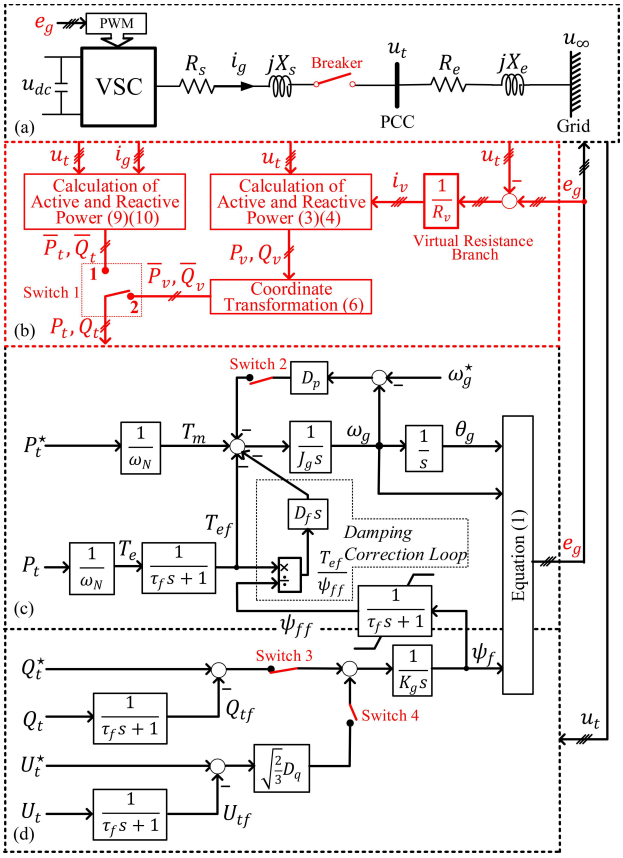

Fig. 1. Proposed self-synchronizing synchronverter. It achieves self synchronization quickly and has few parameters that require tuning. Highlighted in red colour are aspects of particular relevance to the proposed design. (a) Grid interface. (b) Power computation block. (c) Active-power loop. (d) Reactive-power loop.

virtual power feedback signals. Furthermore, the proposed controller adopts the damping correction loop in [6], which enables free adjustment of system damping, and consequently accelerates voltage phase-angle synchronization. These features ensure that the proposed design achieves fast self synchronization with fewer parameters that require tuning. Notably, the virtual resistance branch and the damping correction loop each has only one tuneable parameter. Moreover, the impact of these parameters on the self-synchronization process is well defined (see Section III-B), which facilitates their tuning.

II. Proposed Synchronverter Design

The proposed self-synchronizing synchronverter is connected to the point of common coupling (PCC) via a L-type filter $R_s + jX_s$ and a breaker, as shown in Fig. 1. The external grid, which is connected to the PCC, is modelled as a voltage source u_∞ behind impedance $R_e + jX_e$. The proposed synchronverter controller consists of the power computation block (Fig. 1(b)), the active-power loop (APL) (Fig. 1(c)), and the reactive-power loop (RPL) (Fig. 1(d)). The power computation block returns active- and reactive-power feedback signals, i.e., P_t and Q_t, for the APL and RPL. The APL regulates the synchronverter active-power output P_t to $P_t^\star$ *or* achieves frequency-droop control by adjusting its rotating speed ω_g and rotor angle θ_g, and the RPL tracks the synchronverter reactive-power output Q_t to $Q_t^\star$ *or* achieves voltage-droop control by changing its excitation flux ψ_f. Specifically, self synchronization is achieved by (i) deactivating both frequency- and voltage-droop controls and (ii) regulating both P_t and Q_t to zero. This ensures that the synchronverter inner voltage e_g closely tracks the grid-side voltage u_t before connection to the grid, so that potentially large start-up currents are avoided when the breaker in Fig. 1(a) closes to begin normal operation.

Below, we focus on the power computation block, which includes our key design point, i.e., the virtual resistance branch, followed by the APL and the RPL. We first note that the synchronverter inner voltage e_g is obtained by combining ω_g and θ_g from the APL and ψ_f from the RPL, as follows:

$$e_g = \omega_g \psi_f \left[\sin\theta_g \quad \sin\left(\theta_g - \tfrac{2\pi}{3}\right) \quad \sin\left(\theta_g + \tfrac{2\pi}{3}\right)\right]^{\mathrm{T}}, \quad (1)$$

and its corresponding voltage line-to-line RMS value is $E_g = \sqrt{3/2}\omega_g\psi_f$.

A. Power Computation Block

In the power computation block, as shown in Fig. 1(b), instead of the conventional virtual impedance branch $(\widetilde{L}_v s + \widetilde{R}_v)^{-1}$, we propose to use only a virtual resistance. The virtual resistance avoids dynamics arising from the virtual inductance in $(\widetilde{L}_v s + \widetilde{R}_v)^{-1}$, which slightly slow down the self-synchronization process. Moreover, unlike $(\widetilde{L}_v s + \widetilde{R}_v)^{-1}$ that has two parameters that require tuning, the virtual resistance branch has only one and so the tuning procedure is simplified. During self synchronization, the breaker in Fig. 1(a) is open, and the actual synchronverter active- and reactive-power outputs, $\overline{P}_t$ and $\overline{Q}_t$, are both zero. In order to ensure that the inner voltage e_g closely tracks u_t, the power computation block provides the APL and RPL with feedback signals P_t and Q_t that result from their virtual analogues P_v and Q_v. To achieve this, turn Switch 1 in Fig. 1(b) to position 2. In this way, virtual currents i_v flowing through the virtual resistance R_v are obtained as

$$i_v = (e_g - u_t)/R_v, \quad (2)$$

where $i_v = [i_{va},\ i_{vb},\ i_{vc}]^{\mathrm{T}}$ and the measured PCC voltage $u_t = [u_{ta},\ u_{tb},\ u_{tc}]^{\mathrm{T}}$. With i_v and u_t in place, we define virtual active and reactive power as [10],

$$P_v = u_{ta} i_{va} + u_{tb} i_{vb} + u_{tc} i_{vc}, \quad (3)$$

$$Q_v = \frac{(u_{ta} - u_{tb}) i_{vc} + (u_{tb} - u_{tc}) i_{va} + (u_{tc} - u_{ta}) i_{vb}}{\sqrt{3}}. \quad (4)$$

Suppose that u_∞ is a balanced three-phase voltage, as is u_t because $u_t = u_\infty$ when the breaker is open. Let U_∞ and θ_∞ denote the line-to-line RMS value and the phase angle of u_∞, and define $\theta_{g\infty} := \theta_g - \theta_\infty$ as the phase-angle difference between e_g and u_∞. Then, P_v and Q_v also satisfy [11]

$$P_v = \frac{E_g U_\infty}{R_v}\cos\theta_{g\infty} - \frac{{U_\infty}^2}{R_v}, \quad Q_v = -\frac{E_g U_\infty}{R_v}\sin\theta_{g\infty}, \quad (5)$$

which suggest that P_v and Q_v are, respectively, closely related to E_g and $\theta_{g\infty}$. This is because we only have a virtual

resistance, not a virtual impedance (which is predominantly inductive). However, the APL and RPL are designed for predominantly inductive grid conditions, i.e., the APL input P_t and RPL input Q_t are, respectively, regulated by the rotor angle θ_g and the inner voltage magnitude E_g (or the excitation flux ψ_f). Thus, during self synchronization, P_v and Q_v cannot be directly used as the APL and RPL inputs. To ensure that P_t and Q_t are still regulated by $\theta_{g\infty}$ and E_g, respectively, we utilize the following coordinate transformation:

$$\begin{bmatrix} \overline{P}_v \\ \overline{Q}_v \end{bmatrix} = \begin{bmatrix} 0 & -1 \\ 1 & 0 \end{bmatrix} \begin{bmatrix} P_v \\ Q_v \end{bmatrix} =: T_r \begin{bmatrix} P_v \\ Q_v \end{bmatrix}. \tag{6}$$

The post-transformation variables $\overline{P}_v$ and $\overline{Q}_v$ are subsequently used as the APL and RPL inputs, i.e.,

$$P_t = \overline{P}_v = \frac{E_g U_\infty}{R_v} \sin\theta_{g\infty}, \tag{7}$$

$$Q_t = \overline{Q}_v = \frac{E_g U_\infty}{R_v} \cos\theta_{g\infty} - \frac{{U_\infty}^2}{R_v}. \tag{8}$$

Here, we make two key observations. First, T_r in (6) is a rotation matrix and corresponds to a $\pi/2$ planar rotation counterclockwise about the origin [11]. Second, the resultant (7) and (8) suggest that P_t and Q_t are, respectively, regulated by $\theta_{g\infty}$ and E_g. In fact, via the coordinate transformation in (6), the virtual resistance R_v acts equivalently as a reactance for the purpose of computing virtual power feedback signals, but without inductance dynamics. The equivalent system during self synchronization is shown in Fig. 2. The proposed design avoids the inductance dynamics present in the virtual impedance branch and accelerates the self-synchronization. Also, we only need to tune one parameter R_v in the virtual resistance branch, instead of two in the virtual impedance case.

Once e_g is synchronized with u_t, we may close the breaker and turn Switch 1 to position 1. The self-synchronization process ends, and the synchronverter is connected to the grid and operates normally. During normal operation, the feedback active and reactive powers represent the actual converter outputs and are, respectively, computed according to [10]

$$P_t = \overline{P}_t = u_{ta} i_{ga} + u_{tb} i_{gb} + u_{tc} i_{gc}, \tag{9}$$

$$Q_t = \overline{Q}_t = \frac{(u_{ta} - u_{tb}) i_{gc} + (u_{tb} - u_{tc}) i_{ga} + (u_{tc} - u_{ta}) i_{gb}}{\sqrt{3}}, \tag{10}$$

where $i_g = [i_{ga},\ i_{gb},\ i_{gc}]^{\mathrm{T}}$ is the actual current flowing from the VSC into the grid.

B. Active- and Reactive-power Loops

During self synchronization, the APL and RPL, respectively, synchronize the phase angle and voltage magnitude by regulating P_t and Q_t to zero. Below, we describe the APL and RPL in detail.

1) Active-power loop: During self synchronization, the APL synchronizes the phase angle of e_g to that of u_∞, i.e., it ensures that the angle difference $\theta_{g\infty} = 0$. As depicted in Fig. 1(c), the APL emulates the synchronous generator rotor dynamics and regulates the synchronverter active-power

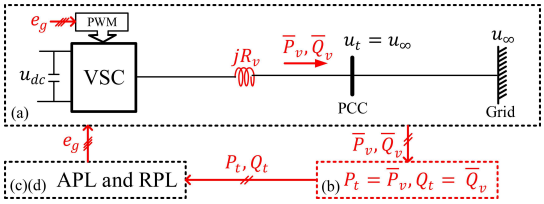

Fig. 2. Equivalent representation of proposed synchronverter design in Fig. 1 during self synchronization (Switch 1 in Fig. 1(b) is at position 2). (a) Virtual equivalent grid interface corresponding to Figs. 1(a) and 1(b), in which R_v equivalently acts as virtual reactance jR_v according to (7) and (8), obtained via the coordinate transformation in (6). (b) Active- and reactive-power feedback signals. (c)(d) APL and RPL.

output P_t. Let T_{ef} and ψ_{ff}, respectively, denote the filtered electromagnetic torque and the filtered excitation flux. Also let S_i represent the state of Switch i (if Switch i is closed, $S_i = 1$, and if Switch i is open, $S_i = 0$, $i = 2, 3, 4$). Then, the APL dynamics are described by [6]

$$J_g \frac{d\omega_g}{dt} = T_m - T_{ef} - S_2 D_p(\omega_g - \omega_g^\star) - D_f \frac{d}{dt}\left(\frac{T_{ef}}{\psi_{ff}}\right), \tag{11}$$

where J_g denotes the inertia constant and $\omega_g^\star$ the reference value of ω_g. In (11), the input torque is $T_m = P_t^\star/\omega_N$, where $P_t^\star$ is the active-power reference and ω_N is the rated rotating angular speed. The term $S_2 D_p(\omega_g - \omega_g^\star)$ is the switchable power-frequency droop control. The term $D_f \frac{d}{dt}\left(\frac{T_{ef}}{\psi_{ff}}\right)$ represents the damping correction loop, which adjusts the synchronverter damping torque during transients prior to reaching steady state but does not affect the steady-state performance [6]. Note that the rotor angle θ_g is obtained by integrating ω_g over time, i.e., $\theta_g = \int_0^t \omega_g(\tau) d\tau$. In (11), T_{ef} and ψ_{ff} are obtained from

$$\tau_f \frac{dT_{ef}}{dt} = -T_{ef} + T_e, \quad \tau_f \frac{d\psi_{ff}}{dt} = -\psi_{ff} + \psi_f, \tag{12}$$

where $T_e = P_t/\omega_N$ is the electromagnetic torque and τ_f is the time constant of low-pass filters (LPFs). During self synchronization, we open Switch 2 ($S_2 = 0$), and set $P_t^\star$ to be zero. In this way, we can regulate $P_t = \overline{P}_v$ to be zero with no steady-state offset, and according to (7), we have $\theta_{g\infty} = 0$. That is, the phase angle of e_g is synchronized with that of u_∞.

2) Reactive-power loop: During self synchronization, the RPL synchronizes the magnitude of e_g to that of u_∞, i.e., it ensures that $E_g = U_\infty$. As shown in Fig. 1(d), depending on the states of Switches 3 and 4, the RPL can regulate the synchronverter reactive-power output Q_t *or* the line-to-line RMS value U_t of the voltage u_t at the PCC. The RPL dynamics are described as follows:

$$K_g \frac{d\psi_f}{dt} = S_3(Q_t^\star - Q_{tf}) + S_4\sqrt{\frac{2}{3}}(U_t^\star - U_{tf}), \tag{13}$$

where K_g is a tuneable parameter, and $Q_t^\star$ and $U_t^\star$ are the reference values of Q_t and U_t, respectively. In (13), Q_{tf} and U_{tf} are filtered signals obtained by

$$\tau_f \frac{dQ_{tf}}{dt} = -Q_{tf} + Q_t, \quad \tau_f \frac{dU_{tf}}{dt} = -U_{tf} + U_t. \tag{14}$$

TABLE I
PARAMETERS OF SYNCHRONVERTER-CONNECTED SYSTEM

Parameters	Method A	Method B	Method C
J_g [kg · m^2]	2.81	2.81	2.81
τ_f [s]	0.0100	0.0100	0.0100
K_g [$\frac{\text{Var}\cdot\text{rad}}{\text{V}}$]	9000	10000	200000
R_v [Ω]	5.00	0.500	1.80
D_f [$\frac{\text{V}\cdot\text{s}}{\text{rad}}$]	7.00	0.500	—
L_v [H]	—	0.0130	0.00300
k_p	—	—	2.00×10^{-4}
k_i	—	—	1.00×10^{-5}

During self synchronization, Switch 3 is closed ($S_3 = 1$), Switch 4 is open ($S_4 = 0$), and $Q_t^\star$ is set as zero. In this way, we regulate the reactive power Q_t to be $Q_t^\star = 0$ with no steady-state error. Note that we usually tune the APL to respond more quickly than the RPL, which ensures that $\theta_{g\infty}$ converges to 0 sooner. Thus, according to (8), we have that $E_g = U_\infty$ when $Q_t = \overline{Q}_v = 0$. That is, the magnitude of e_g is synchronized with that of u_∞. Note that if the synchronverter were to supply local loads during self synchronization, as in [12], we would first use u_∞ as the synchronverter modulation signal, and then switch to e_g when $e_g = u_\infty$.

For self synchronization, the proposed synchronverter has only three parameters that require tuning by trial and error: R_v, D_f, and K_g. The remaining parameters, i.e., τ_f and J_g, are set to be the same as their values in normal operation status. This represents an improvement over existing designs, e.g., [5] and [6], which have four or more parameters that need to be tuned by trial and error. In the next section, we validate that the proposed design achieves self synchronization quickly and that its controller parameters can be tuned easily.

III. CASE STUDIES

In this section, via numerical simulation studies, we first verify that the proposed self-synchronizing synchronverter can achieve self synchronization more quickly than other conventional designs. Then, we show that increasing D_f and decreasing K_g, respectively, accelerate the voltage phase angle and magnitude synchronization process. In so doing, we show that the proposed design significantly simplifies the parameter tuning process. The simulated system in Fig. 1 is modelled in PSCAD/EMTDC with grid interface parameters chosen as follows: $R_s = 0.741\ \Omega$, $L_s = 20.0$ mH, $R_e = 0.00\ \Omega$, $L_e = 38.5$ mH, $U_\infty = 6.60$ kV, and the grid frequency is $f_\infty = 60$ Hz.

A. Validating Self-synchronzation Speed

In this case study, via numerical simulations, we show that the proposed controller design (method A) achieves faster self-synchronization speed than two existing methods in [6] (method B) and [5] (method C). Method B adopts a virtual impedance branch consisting of $(\widetilde{L}_v s+\widetilde{R}_v)^{-1}$ with inductance dynamics, and method C achieves phase-angle synchronization with an additional PI controller $k_p + k_i/s$ instead of the damping correction loop in our proposed method A. We tune controller parameters for methods A, B, and C via trial and error until, to the best of our abilities, each method achieves self synchronization as quickly as possible. The chosen parameters for methods A, B, and C are reported in Table I, columns 2, 3, and 4, respectively. For method C, we also initialize the excitation flux ψ_f to be 14 Wb in order to accelerate its self-synchronization process and to ensure large-signal system stability, since this value corresponds to the grid voltage U_∞ used in the simulations. On the other hand, in methods A and B, we set $\psi_f = 0.01$ Wb at $t = 0$ s. In other words, we do not need to initialize ψ_f according to the grid voltage.

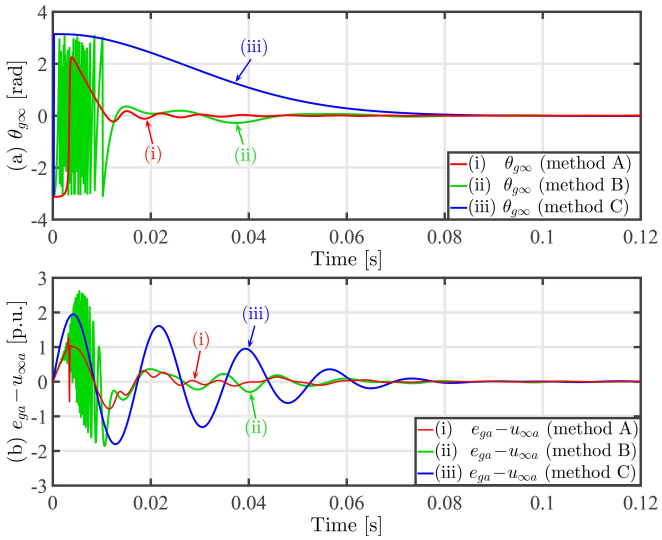

Fig. 3. Comparison of self-synchronization speeds when adopting the proposed method (method A), the method in [6] (method B), and the method in [5] (method C). Method A achieves self-synchronization more quickly than methods B and C.

1) Scenario 1: Self synchronization begins at $t = 0$ s and the breaker remains open. Simulation results of methods A, B, and C are presented in Fig. 3. In order to compare the self-synchronization speeds of these methods, we consider an extreme case, where the initial phase-angle difference $\theta_{g\infty}$ between e_g and u_∞ is π [rad] at $t = 0$ s. As shown in Fig. 3(a), during self synchronization, all three methods ensure that $\theta_{g\infty}$ converges to zero, i.e., synchronizing the phase angle of e_g to that of u_∞. Via visual inspection of Fig. 3, we find that method A (trace (i)) achieves phase-angle synchronization most quickly, taking about 0.04 s. Figure 3(b) plots the difference between e_{ga} and $u_{\infty a}$, which are, respectively, the a-phase instantaneous values of e_g and u_∞. We find that $(e_{ga} - u_{\infty a})$ decreases to zero in all three methods. The convergence speeds are similar for methods A and B, while method C is slower. The initial transient oscillations in trace (ii) (method B) in both Figs. 3(a) and (b) result from the inductance dynamics in the virtual impedance branch, and these transient cause method B to be slightly slower than method A. Note that in Fig. 3(b), trace (i) (method A) contains a sharp dip at $t = 0.0035$ s. Here, ω_g takes a very large value (also reflected in the abrupt increase in trace (i) of Fig. 3(a)), which causes the magnitude of e_g to be large, according to (1).

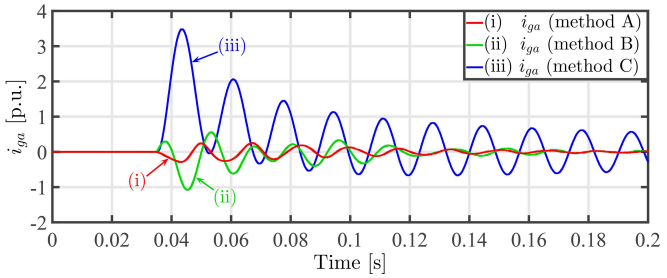

Fig. 4. Comparison of the a-phase start-up currents i_{ga} with method A, B, and C when connecting the synchronverter to the grid at $t = 0.035$ s. With method A, the start-up current after $t = 0.035$ s is minimal, since method A achieves self synchronization most quickly.

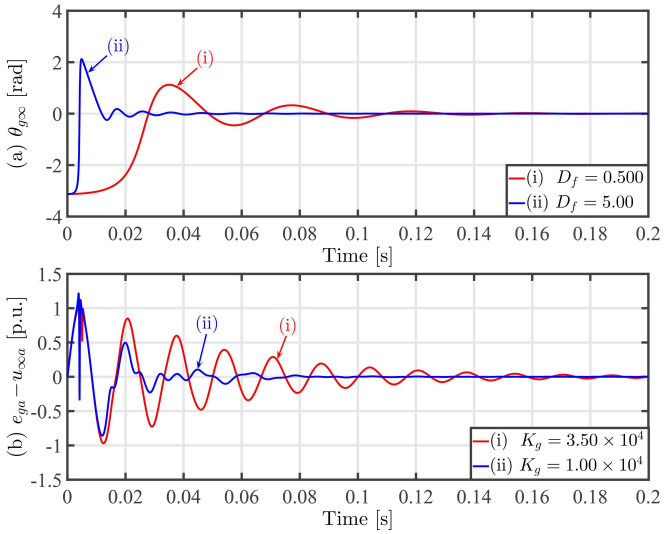

Fig. 5. Validating that increasing D_f and reducing K_g, respectively, accelerate the voltage phase-angle and magnitude self-synchronization process. (a) Effect of D_f on phase-angle synchronization ($K_g = 1.0 \times 10^4$ $\frac{\text{Var}\cdot\text{rad}}{\text{V}}$). (b) Effect of K_g on self synchronization ($D_f = 5.00$ $\frac{\text{V}\cdot\text{s}}{\text{rad}}$).

2) Scenario 2: Here, suppose that self synchronization begins at $t = 0$ s, but we close the breaker at $t = 0.035$ s, and afterwards, let $P_t^\star$ and $Q_t^\star$ remain zero. The a-phase start-up current i_{ga} with methods A, B, and C are shown in Fig. 4. We find that the start-up current i_{ga} corresponding to method A (trace (i)) is minimal. This also validates that method A synchronizes e_g to u_∞ more quickly than methods B and C.

In summary, the proposed design (method A) self synchronizes more quickly than methods B and C, because method A does not suffer from inductance dynamics that delay the synchronization process in methods B and C. Also, Method A adopts the damping correction loop, which accelerates phase-angle self synchronization.

B. Validating the Controller Parameters to be Easily Tuneable

In this case study, we show that the parameters of the proposed controller design are easily tuneable. Recall that we need to tune R_v, D_f, and K_g via trial and error. First, we choose a positive value for R_v, e.g., $R_v = 5.00\ \Omega$. Among the remaining two parameters D_f and K_g, if we increase D_f from 0.50 to $5.00\ \text{V}\cdot\text{s/rad}$, as shown in Fig. 5(a), $\theta_{g\infty}$ converges to zero more quickly. In other words, increasing D_f would accelerate the phase-angle self-synchronization process. This is because the APL has larger damping when D_f is greater. For K_g, decreasing its value would accelerate the voltage-magnitude self-synchronization process. For example, as shown in Fig. 5(b), reducing K_g from 3.5×10^4 to 1.00×10^4 $\text{Var}\cdot\text{rad/V}$ results in faster convergence of the magnitude of $(e_{ga} - u_{\infty a})$ to zero. This is because according to (13), the RPL responds more quickly with smaller K_g. Although we need to tune R_v, D_f, and K_g via trial and error, the impacts of D_f and K_g on the self-synchronization dynamic process are clear and well defined, as explained above. Thus, we conclude that the parameters of the proposed self-synchronizing synchronverter are easily tuneable. Since the choices for R_v, D_f, and K_g influence each other, the resulting parameter values may not be unique.

IV. Concluding Remarks

This paper proposes a self-synchronizing synchronverter design that uses a virtual resistance branch and the damping correction loop. The virtual power feedback signals are computed via a coordinate transformation to ensure expected operation of APL and RPL during self synchronization. The proposed design not only achieves self synchronization more quickly than existing designs, but also has fewer parameters that need to be tuned via trial and error. The proposed controller design can be widely adopted in applications like grid connection of RESs, HVDC links, and static compensators.

References

[1] D. Dong, B. Wen, D. Boroyevich, P. Mattavelli, and Y. Xue, "Analysis of phase-locked loop low-frequency stability in three-phase grid-connected power converters considering impedance interactions," *IEEE Trans. Ind. Electron.*, vol. 62, no. 1, pp. 310–321, Jan. 2015.

[2] H. P. Beck and R. Hesse, "Virtual synchronous machine," in *Proc. 9th Int. Conf. Elect. Power Quality Util.*, 2007, pp. 1–6.

[3] Q.-C. Zhong and G. Weiss, "Synchronverters: Inverters that mimic synchronous generators," *IEEE Trans. Ind. Electron.*, vol. 58, no. 4, pp. 1259–1267, Apr. 2011.

[4] W. Zhang, D. Remon, I. Candela, A. Luna, and P. Rodriguez, "Grid-connected converters with virtual electromechanical characteristics: experimental verification," *CSEE Journal of Power and Energy Systems*, vol. 3, no. 3, pp. 286–295, Sep. 2017.

[5] Q.-C. Zhong, P. L. Nguyen, Z. Ma, and W. Sheng, "Self-synchronized synchronverters: Inverters without a dedicated synchronization unit," *IEEE Trans. Power Electron.*, vol. 29, no. 2, pp. 617–630, Feb. 2014.

[6] S. Dong and Y. C. Chen, "Adjusting synchronverter dynamic response speed via damping correction loop," *IEEE Trans. Energy Convers.*, vol. 32, no. 2, pp. 608–619, Jun. 2017.

[7] M. Amin, A. Rygg, and M. Molinas, "Self-synchronization of wind farm in an MMC-based HVDC system: A stability investigation," *IEEE Trans. Energy Convers.*, vol. 32, no. 2, pp. 458–470, 2017.

[8] Q.-C. Zhong, W. L. Ming, and Y. Zeng, "Self-synchronized universal droop controller," *IEEE Access*, vol. 4, pp. 7145–7153, Oct. 2016.

[9] O. Mo, S. D'Arco, and J. A. Suul, "Evaluation of virtual synchronous machines with dynamic or quasi-stationary machine models," *IEEE Trans. Ind. Electron.*, vol. 64, no. 7, pp. 5952–5962, Jul. 2017.

[10] H. Akagi, E. H. Watanabe, and M. Aredes, *Instantaneous power theory and applications to power conditioning*. Piscataway, NJ: IEEE Press, 2007.

[11] K. D. Brabandere, B. Bolsens, J. V. den Keybus, A. Woyte, J. Driesen, and R. Belmans, "A voltage and frequency droop control method for parallel inverters," *IEEE Trans. Power Electron.*, vol. 22, no. 4, pp. 1107–1115, Jul. 2007.

[12] C. Verdugo, J. I. Candela, and P. Rodriguez, "Re-synchronization strategy for the synchronous power controller in hvdc systems," in *Proc. Energy Convers. Congr. Expo.*, Oct. 2017, pp. 5186–5191.